A new algorithm for detecting trophic status (chlorophyll-a), cyanobacterial-dominanance, surface scums and floating vegetation in coastal and inland waters from MERIS

Mark William Matthews[a], Stewart Bernard[b,a], Lisl Robertson[b]

[a]*Marine Remote Sensing Unit, Department of Oceanography, University of Cape Town, Rondebosch, 7701, Cape Town, South Africa*

[b]*Earth Systems Earth Observation, Council for Scientific and Industrial Research, 15 Lower Hope Street, Rosebank, 7700, Cape Town, South Africa*

Abstract

A novel algorithm is presented for detecting trophic status (chlorophyll-*a*), cyanobacterial blooms (cyano-blooms), surface scum and floating vegetation in coastal and inland waters using top-of-atmosphere data from the Medium Resolution Imaging Spectrometer (MERIS). The Maximum Peak Height algorithm (MPH) uses a baseline subtraction procedure to calculate the height of the dominant peak across the red and near-infrared (NIR) MERIS bands between 664 and 885 nm caused by sun-induced chlorophyll fluorescence (SICF) and particulate backscatter. Atmospheric correction of the MERIS TOA reflectance data for gaseous absorption and Rayleigh scattering proved adequate given the spectral proximity of the relevant bands and the sufficiently large differential spectral signal. This avoided the need to correct for atmospheric aerosols, a procedure which is typically prone to large errors in turbid and high-biomass waters. A combination of switching algorithms for estimating chl-a were derived from coincident *in situ* chl-*a* and MERIS bottom-of-rayleigh reflectance measurements. These algorithms are designed to simultaneously handle a wide trophic range, from oligotrophic/mesotrophic waters (chl-*a* < 20 mg.m^{-3}), to eutrophic/hypertrophic waters (chl-*a* > 20 mg.m^{-3}) and surface scums or dry floating algae or vegetation (dystrophic, chl-*a* > 500 mg.m^{-3}). In addition, cyanobaceria-dominant waters were differentiated from those dominated by prokaryote species (dinoflagellates/diatoms) on the basis of the magnitude of the MPH variable. This is supported by evidence that vacuolate cyanobacteria (e.g. *Microcystis aeruginosa*) possess enhanced chl-*a* specific backscatter which is an important bio-optical distinguishing feature. This enables these broad algal classes to be distinguish with some certainty from space. A flag based on cyanobacteria-specific spectral pigmentation and fluorescence features was also used to identify cyanobacterial dominance in eutrophic waters. An operational algorithm for use with prokaryote-algae for chl-*a* in the range $0.5 - 350.4$ mg.m^{-3} gave a coefficient of determination of 0.71 and a mean absolute percentage error (mape) of 60% (N=48). An algorithm for cyano-dominant waters had an r^2 of 0.58 for chl-*a* between 33 and 362.5 mg.m^{-3} and an error of 33.7% (N=17). Example applications demonstrate how the MPH algorithm can offer rapid and effective assessment of trophic status, cyano-blooms, surface scums and floating vegetation in inland and coastal waters.

Keywords: Trophic status, eutrophication, water quality, cyanobacterial-dominance, cyanobacteria, surface scums, floating vegetation, MERIS, southern Africa, optical remote sensing, chlorophyll-*a*, Benguela, Hartbeespoort, Zeekoevlei, Loskop

1. Introduction

The needs of near-coastal and inland users are generally not addressed by global ocean colour algorithms, which primarily have an open-ocean focus and are not designed for the predominance of case II and eutrophic waters encountered in close proximity to land. User needs for such waters are typically focused on water quality rather than biogeochemistry, and a greater emphasis is placed on the use of earth observation data for sustainable resource management; operational detection of trophic state, and phenological characterization of eutrophication over time as a primary longer-term research goal. The optical complexity and sometimes extreme concentration of constituents in these coastal and inland waters calls for new atmospheric and bio-optical scientific capabilities; whilst the shift in scientific application calls for new and more applied product types such as eutrophication indices. The Medium Resolution Imaging Spectrometer (MERIS), and the planned OLCI sensor on the Sentinel 3 platforms, are likely the current and planned optimal sensors for near real-time frequent monitoring applications for spatially constrained inland and transitional coastal waters (Guanter et al., 2010; Matthews, 2011). Chlorophyll a (chl-*a*) algorithms for MERIS in turbid, high-biomass inland and coastal waters have historically been based on the water-leaving reflectance (Gons et al., 2002; Gons, 2005; Gitelson et al., 2008, 2009; Moses et al., 2009a,b). However, the limited ability of routinely implemented atmospheric corrections for accurately resolving the shape of the water-leaving reflectance in the red-NIR MERIS bands in high biomass bright-pixel waters, has hampered these efforts (Schiller & Doerffer, 2005; Guanter et al., 2010; Matthews et al., 2010). Here, for the first time, a novel red-edge baseline-subtraction algorithm is presented for retrieving phytoplankton abundance estimates (chl-*a*) directly from MERIS bottom-of-rayleigh reflectance (BRR) in low and high biomass phytoplankton-abundant inland and coastal waters. The algorithm is named the Maximum Peak Height or MPH algorithm, because it switches to exploit the position and magnitude of the chl-*a* fluorescence and particulate backscatter/absorption related peaks in the MERIS red/NIR bands. The top-of-atmosphere (TOA) approach used by the MPH avoids error-prone aerosol atmospheric correction procedures used to derive the water leaving reflectance, while the algorithms baseline-subtraction calculation effectively normalizes for atmospheric effects. The MPH is derived from coincident measurements of *in situ* chl-*a* and MERIS reflectance in four diverse phytoplankton-abundant southern African systems. These are the southern Benguela marine coastal upwelling system, and the three inland freshwater reservoirs of Zeekoevlei, Hartbeespoort dam and Loskop dam. The MPH is designed to provide a quantitative measure of trophic status through chl-*a* estimates. It simultaneously handles a wide trophic range, from oligotrophic (chl-*a* < 10) through to dystrophic (chl-*a* > 300) waters, while also offering the ability to identify surface scums and floating vegetation. A method is proposed that enables prokaryote and cyano-dominant assemblages to be distinguished based on the magnitude of the MPH variable and a flag using reflectance features related to chl-*a* and phycocyanin fluorescence. The MPH algorithm is intended for operational trophic status determination, and for providing early warning indicators for cyanobacteria and HABs in phytoplankton-dominant coastal and inland systems. The study continues with a thorough description and error assessment of the datasets used for algorithm derivation, then provides details on the MPH algorithm, and concludes with example applications of the MPH algorithm in various local and global systems.

2. Description of study areas

The MPH was derived using datasets collected from four diverse study areas. The four systems are similar with regard to phytoplankton abundance and the occurrence of HABs, but naturally differ considerably with regards their phytoplankton community structure, biochemistry and ecological drivers. The southern Benguela is an extremely dynamic and productive upwelling system off the west coast of southern Africa that is affected by frequent HAB events (Pitcher & Calder, 2000). In bloom conditions, the phytoplankton assemblage is typically composed of a variety of dinoflagellate or diatom species varying in toxicity, or autrophic ciliates such as *Mesodinium rubrum* (Fawcett et al., 2007). The optical water type can be described as an extreme Case 1, with phytoplankton being the dominant causal IOP, and minerals and gelbstoff playing lesser roles (Bernard et al., 2001). In the Benguela, the concentration of chl-*a* is extremely variable, and may range from less than one mg.m^{-3} in non-bloom conditions, to greater than 500 mg.m^{-3} in peak bloom conditions (Pitcher & Weeks, 2006). Therefore, the southern Benguela represents an extremely variable coastal upwelling system, and a challenging environment for ocean colour remote sensing.

Loskop dam is the most similar of the three inland waters to the Benguela with regards to water type and algal assemblage composition. Located at about 1000 m asl in South Africa's Mpumalanga province 150 km north east of Johannesburg, the lake shows pronounced longitudinal zonation with riverine, transitional and lacustrine zones that range from hypertrophic to oligotrophic, respectively (Oberholster et al., 2010). During winter sampling in July/August of 2011, the riverine zone was dominated by a dense bloom of the large celled dinoflagellate, *Ceratium hirundinella*, which turned the water a chocolate brown colour. Chl-*a* values of up to 500 mg.m^{-3} were recorded in this bloom. In the transitional and lacustrine zones further downstream, lower biomass blooms of chlorophytes and diatoms were present. Chl-*a* values were near 20 mg.m^{-3} in the mesotrophic transitional zone, and less than one mg.m^{-3} in the oligotrophic main basin representing the lacustrine zone. Importantly, dense blooms of the cyanobacteria *Microcystis aeruginosa* become dominant in the riverine and transitional zones in summer months as the water temperature increases. These are present alongside prokaryote species during these months. Additional measurements found that there were also significant contributions from gelbstoff and minerals, indicating a case 2 water type (Matthews, unpublished).

The final two study areas, Zeekoevlei lake and Hartbeespoort dam, represent two of the most productive freshwater reservoirs in southern Africa, and indeed the world (Harding, 1997; Robarts & Zohary, 1984). Their phytoplankton assemblages are near-permanently dominated by the colonial cyanobacterium *Microcystis aeruginosa* and regularly exhibit dense surface blooms called hyperscums (Zohary, 1985). Chl-*a* values in these systems average around 200 mg.m^{-3}, with values in excess of 1000 mg.m^{-3} being frequently recorded. Despite the similar trophic status and phytoplankton assemblages, the two systems differ considerably in their morphology and limnology. Zeekoevlei Lake, located at 5 m asl south of the City of Cape Town in the Western Cape province, is a small (2.5 km^2), shallow (average depth of 2 m) and continuously mixed (hypermictic) naturally occurring freshwater pan. Hartbeespoort dam is by comparison larger (20 km^2), deeper (average depth of 10 m), monomictic and stratified, and is at an altitude of around 1000 m asl in the Highveld province of Gauteng. Despite these differences, the bulk IOPs of both lakes are overwhelmingly dominated by phytoplankton and detrital material (Matthews et al., 2010, unpublished). However, significant contributions by minerals and gelbstoff means that the lakes are by strict definition case 2 waters.

3. Data sets and uncertainties

3.1. Chl-a measurements

3.1.1. Description of combined in situ chl-a dataset

The combined data set consists of 74 *in situ* surface chl-a measurements with corresponding simultaneously acquired MERIS full resolution (FR) or reduced resolution (RR) radiometry as follows: Benguela (N=37), Loskop (N=20), Zeekoevlei (N=9) and Hartbeespoort (N=8). The chl-*a* data from the four systems were acquired through numerous fieldwork campaigns spanning a period of 9 years from 2003 - 2011. In all circumstances, surface water samples were collected from a small boat with care being taken to minimise disturbance of the delicate surface blooms (if present). Chl-*a* was determined using a different analytical technique in each of the study areas. For the Benguela chl-*a* was measured by fluorometric analysis using 90% acetone (Holm-Hansen et al., 1965) in accordance with accepted marine protocols (Ducklow & Dickson, 1994). For inland waters, spectrophotometric analyses with 90% or 95% boiling ethanol was used due to the improved extraction efficiency of ethanol with blue-green algae dominated assemblages (Sartory & Grobbelaar, 1984). Inevitably there will be differences between the extraction efficiencies of the solvents, and between the detection limits of the fluorometric and spectrophotometric techniques. However, no attempt was made to quantify these errors and they are likely to be small compared to the relative standard error of measurement. With the exception of the Benguela dataset, all chl-*a* analyses were performed in triplicate, using the mean as the representative value. The mean relative standard error (mrse) for chl-*a* was calculated as the standard deviation of triplicate results divided by the mean of the triplicate results. In this way, the mrse was determined as 17.1% (N = 31) for Zeekoevlei, 6.5% (N=38) for Hartbeespoort and 29.7% (N=54) for Loskop. It is important to consider the high frequency (> 50%) of low chl-*a* values (< 10 mg.m^{-3}) for the Loskop dataset, leading to larger relative errors. In the absence of triplicate measurements, an mrse of 15% was used for the Benguela.

3.1.2. Error in chl-a due to bloom patchiness: single-point sampling error

Several authors have questioned the usefulness of single point samples for validating remotely sensed chl-*a* due to bloom patchiness (Galat & Verdin, 1989; Kutser, 2004, 2009). Single point surface samples that neglect the horizontal and vertical components may lead to misrepresentative biomass estimates especially in high biomass waters exhibiting patchy blooms, such as in this dataset. There are also significant dilution effects associated with the disturbance of delicate buoyant surface blooms during sampling. Previous estimates of the horizontal patchiness in cyano-blooms in Hartbeespoort (Robarts & Zohary, 1992) and the Gulf of Finland (Kutser, 2004) show that these errors can exceed two orders of magnitude. This leads to substantial within-pixel variability in chl-*a* values making it difficult to validate chl-*a* values retrieved from remote sensing data using single point samples.

In order to guage the likely relative magnitude of the error due to horizontal and vertical patchiness for the dataset, coincident measurements from a Hyperspectral Tethered Surface Radiometer Buoy (Satlantic Inc.) were used. The TSRB measures the upwelling spectral radiance at a depth of 0.66 m, Lu(0.66), and the downwelling irradiance above the surface, Ed(0+), in the spectral range 400 to 800 nm with a frame rate of 1 Hz, a resolution of 3.3 nm and an accuracy of 0.3 nm. During sampling, the TSRB is allowed to drift freely in the sample area and acquire data for no less than three minutes. This sampling time and drift is considered sufficient to capture bloom patchiness occurring in the sample areas. The relative standard error of the 710 nm band, known to be significantly correlated with chl-*a* values in high phytoplankton biomass waters

(Gitelson, 1992; Schalles et al., 1998), is calculated from the typical three minute burst sampling time and can be used as an approximate index for biomass patchiness. The results indicated that for Hartbeespoort, a highly stratified system with severely patchy cyano-blooms, the error due to bloom patchiness had a mean of 14.8% and a maximum of 44.8% (N=17). For the Benguela, a more mixed system with occasional surface blooms, the mean error is 10.8% (N = 44). For the hypermictic Zeekoevlei the mean error is reduced to only 8.6% (N=18). These mean errors were used as the typical expected error to single point chl-*a* measurements resulting from bloom patchiness for the dataset (patchiness error for Loskop was estimated at 10%).

Therefore, the total uncertainty of *in situ* chl-*a* measurements was calculated by adding the mrse of measurement and the single point sampling error estimates. The total mean expected error for chl-*a* values from single-point surface samples for the four systems are estimated as 39.7% for Loskop, 25.8% for the Benguela, 25.7% for Zeekoevlei and 21.3% for Hartbeespoort. These errors are shown as error bars are on the plots.

3.2. MERIS reflectance data

3.2.1. Data processing and atmospheric correction

MERIS data were processed using the Basic ENVISAT Toolbox for (A)ATSR and MERIS (BEAM) V. 4.9.0.1. The L1b data were first corrected for the SMILE effect, detector-to-detector systematic radiometric differences, and recalibrated using the Level 1 Radiometry Processor V. 1.0.1 (Bouvet & Ramoino, 2009). An improved cloud product was calculated using the Cloud Processor V. 1.5.203 (© ESA, FUB, and Brockmann Consult, 2004). In order to account for the effects of gaseous absorption in the red bands from water-vapour (H_2O), ozone (O3) and molecular Rayleigh scattering, the bottom-of-Rayleigh reflectance processor V. 2.3 was then used to compute the bottom of Rayleigh reflectance data (BRR), or ρ_{BR} (Santer et al., 1999; ACRI, 2006). The simplified atmospheric correction procedure is a first attempt to normalise the TOA signal for gaseous and Rayleigh effects, whilst ignoring the more complicated and variable effects of absorbing aerosols (particles like smoke and dust). Importantly, the procedure corrects for the significant absorption by water vapour in the band centered at 709 nm. For comparison, and to assess the impact of the adjacency effect, the Improve Contrast between Ocean and Land (ICOL+) processor V. 2.6 was also implemented to give the adjacency effect corrected (AEC) BRR reflectance, or ρ_{AECBR} (Santer, 2010). The adjacency effect from Rayleigh scattering and aerosols was computed taking into account the aerosol type over water and case 2 waters.

The limited geographical extent of the inland water bodies in this study necessitates the use of MERIS full resolution (FR) data, whereas in the Benguela FR data are not systematically acquired and reduced resolution (RR) data are more frequently available for routine processing. As a result, a combination of FR (inland) and RR (Benguela) data are used in this study. A comparison of the Level 1 FR and RR data for the pixels of interest was performed in order to assess whether any discrepancies potentially impacted upon the comparative use of FR and RR data. RR pixels are made up of an averaging of 16 (4x4) FR pixels. Due to the complexities of geolocation and the fact that this averaging is done on-board the satellite before any subsetting takes place, it is difficult to select exactly these 16 pixels from a FR image (which is necessarily a subset of the RR image) and manually recreate an existing RR pixel. Instead, a pixel-by-pixel approach was undertaken, and only the pixel closest to the sampling station was selected from each FR and RR image. 8 co-incident FR/RR images, with chl-*a* values ranging from 8 mg.m^{-3} to 172 mg.m^{-3} were used for this experiment. All the images were processed using IPF-5.02 and above. The results showed excellent agreement in the FR/RR radiometry, with relative unsigned

Table 1: Relative unsigned percentage errors in TOA radiances between FR and RR data in all 15 MERIS bands.

λ (nm)	412	442	490	510	560	620	665	681
Error (%)	0.242	0.4372	0.530	0.456	0.870	1.842	1.940	2.373
λ (nm)	709	754	761	779	865	885	900	
Error (%)	4.098	3.140	3.667	3.666	3.922	5.002	5.570	

percentage errors in TOA radiances in all 15 bands shown in Table 1. An overall correlation of $y = x - 0.23$ was observed across all bands (TOA radiances in mW.m^{-2}.sr^{-1}.nm^{-1}), with a slight negative offset in the RR. This can be explained by the averaging process which somewhat dampens localised elevated signals in the higher resolution data. The higher relative percentage errors in the red and NIR are to be expected where the signal is very small. Likewise in the 709 nm region which is very reactive to varying chl-*a* concentrations, a relative error of 4% is quite acceptable given the magnitude of the signal and the increased likelihood of patchiness in the water in high biomass scenarios. The overall error associated with the reflectance based independent variables was determined through error propagation analysis using the combined FR/RR and systematic bias uncertainties. The systematic bias in TOA radiance determined through on-board calibration has been estimated at less than 2% (Sotis, 2007). Therefore, taking account of error propagation, the error from MERIS radiometry in the algorithm was estimated as no greater than 4%.

3.2.2. MERIS bottom-of-Rayleigh reflectance data

MERIS reflectance spectra from single pixels were extracted from processed MERIS scenes corresponding to *in situ* match-up stations. The time difference between the *in situ* surface sample collection and the MERIS overpasses is less than 2 hours (but often less than 30 minutes) for the entire marine and freshwater dataset. Fig. 1 shows the bottom-of-Rayleigh reflectance data for the match-up dataset. The spectra have been arranged to aid comparison of the spectral shapes associated with the different waters, with spectra with fluorescence effects (681 nm) and absorption/backscatter (709 nm) maximum peak positions displayed separately. Fig. 1.A shows spectra from the Benguela with a prominent 681 nm fluorescence peak that are otherwise relatively flat at longer wavelengths towards the NIR. The spectra from Loskop in fig. 1.B have less obvious fluorescence peaks and are noisier towards the NIR, although the magnitudes are very similar to those in fig. 1.A. The spectra in fig. 1.C from Loskop and Benguela have clearly distinguishable peaks at 709 nm and belong to the absorption/backscatter domain. However, there is a clear difference between spectra from the Benguela, which typically slope downwards toward the NIR, and those from Loskop which have a continuous upward slope. The increased NIR reflectance values from Loskop are most likely caused by the adjacency effect in the small inland water body, or even partial contamination of the pixels from nearby land. This effect is also apparent in fig. 1.B. Finally, fig. 1.D presents spectra from the cyanobacteria-dominated waters of Hartbeespoort and Zeekoevlei. Three features specific to fig. 1.D are worth noting: the larger magnitudes of the 709 nm peak relative to fig. 1.C; a marked trough at 681 nm (arrow 1); and a small peak at 664 nm (arrow 2). These features make these spectra unique from those in the other panels. The increased magnitude of the 709 peak is thought to be due to cyanobacterial ultrastructure and is examined in detail in section 4.3. The 681 nm trough (arrow 1) is caused by a reduction in SICF in cyanobacteria dominant waters. Cyanobacteria possess very inefficient SICF as most of the chl-*a* is located in photosystem I (Seppälä et al., 2007). Based on this evidence, a 681 nm fluorescence signal cannot be used for chl-*a* estimation in cyanobacteria

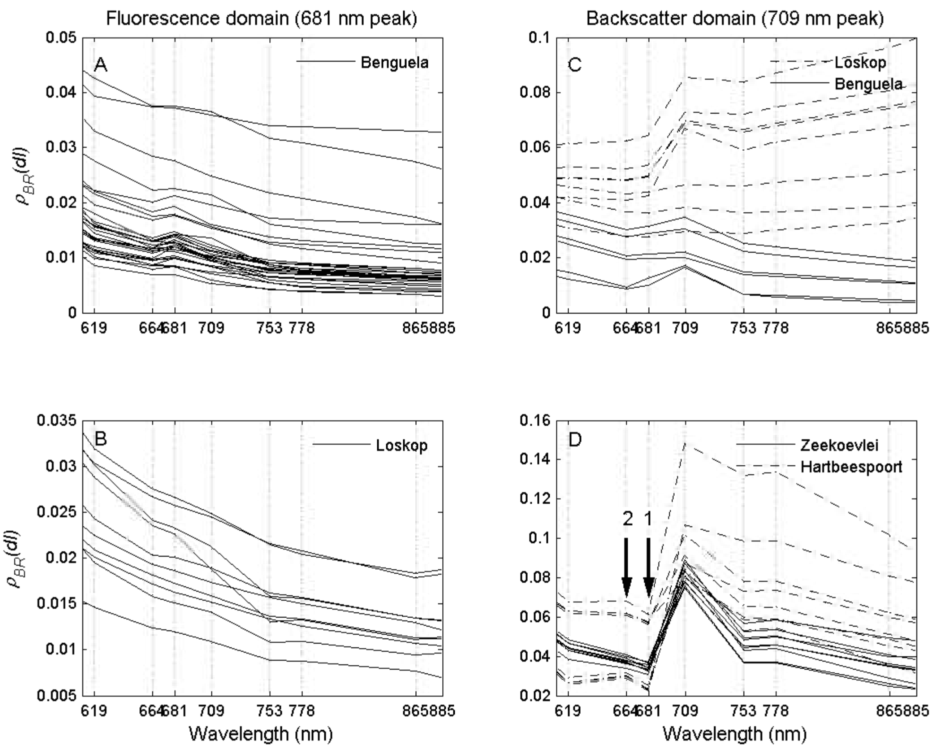

Figure 1: Bottom-of-Rayleigh reflectance spectra from single pixels corresponding to coincident chl-*a* measurements from each of the four study areas as indicated. The left hand side panels (A, B) display spectra possessing a 681 nm fluorescence related maximum peak position, while the right hand side (C, D) those with a 709 nm backscatter related maximum peak position. For more detail see section 3.2.1.

dominant waters. Arrow 2 showing the elevated reflectance in the 664 nm band, overlaps the fluorescence emission domain of the pigment phycocyanin (PC), the main light harvesting pigment in cyanobacterial species (Bogorad, 1975). This sun induced PC fluorescence (SIPF) feature will be shown later to be critical in identifying cyanobacteria-dominant waters (see section 4.4), used in conjunction with the absorption maxima of PC near 620 nm.

4. The MPH algorithm

A modified baseline-subtraction algorithm has been implemented, named the maximum peak height or MPH algorithm (Version 1.0). The MPH is similar in form to the fluorescence line height (FLH) algorithm (Gower et al., 1999). However, instead of having a fixed peak position, the MPH searches for the position and magnitude of the maximum peak in the red/NIR MERIS bands at 681, 709 and 753 nm (bands 8, 9 and 10) caused by either phytoplankton fluorescence or absorption/backscatter. The MPH uses a constant baseline between MERIS bands 7 (664 nm) and 14 (885 nm) to measure the height of the red peak: this constant baseline was found to give more robust results than a spectrally shifting baseline. The MPH is calculated as follows:

$$MPH = \rho_{BRmax} - \rho_{BR664} - ((\rho_{BR885} - \rho_{BR664}) \times (\lambda_{max} - 664)/(885 - 664)) \quad (1)$$

where λ_{max} and ρ_{BRmax} are respectively the position and magnitude of the highest peak in the MERIS bands at 681, 709 and 753 nm.

The MPH is designed to simultaneously handle three cases, each with two sub-cases, commonly occurring in phytoplankton-dominant and HAB affected waters. These can be summarised as follows, and are discussed in detail in the following sections:

1. Mixed oligotrophic/mesotrophic low-medium biomass waters (chl-*a* < 30 mg.m^{-3})
   a) Prokaryote-dominant assemblages with SICF signal (predominantly diatoms/dinoflagellates)
   b) Special case: low biomass cyano-blooms (no observable SICF)
2. High biomass eutrophic/hypertrophic waters (chl-*a* > 30 mg.m^{-3})
   a) Prokaryote-dominant assemblages
   b) Cyanobacteria-dominant assemblages
3. Extremely high biomass (dystrophic, chl-*a* > 500 mg.m^{-3}) with surface scums (hyperscums) or dry floating algae or vegetation
   a) Prokaryote scums (chl-*a* > 500 mg.m^{-3}) and floating aquatic macrophytes
   b) Cyanobacterial scums (chl-*a* > 500 mg.m^{-3})

4.1. Fluorescence domain: mixed oligotrophic/mesotrophic low-medium biomass waters

The first case relates to mixed oligotrophic/mesotrophic low to medium biomass conditions with chl-*a* less than approx. 30 mg.m^{-3}. In these waters where phytoplankton is optically dominant, the concentration of chl-*a* is known to be highly correlated with the line height of the sun-induced chl-*a* fluorescence (SICF) peak at 681 nm (Neville & Gower, 1977; Gower, 1980; Gitelson et al., 1994; Letelier & Abbott, 1996; Hoge et al., 2003; Giardino et al., 2005; Zhao et al., 2008), which is typically larger than the peaks at 709 and 753 nm due to strong absorption by water. In these conditions, the MPH algorithm emulates the fluorescence line height or FLH algorithm Gower et al. (1999), calculating the line height of the fluorescence peak using the MERIS bands 7, 8 and 14. Available validation studies in inland and coastal waters using an FLH type algorithm with MERIS have shown the significant potential of this approach (Gower & King, 2007; Lee et al., 2007; Gons et al., 2008; Binding & Greenberg, 2011). An important distinctionfrom previous studies is that this study demonstrates the ability to detect SICF using a type of TOA reflectance, rather than water-leaving reflectance data. The possibility to detect chl-*a* fluorescence at high altitudes despite atmospheric effects was demonstrated by Neville and Gower (1977) and is further confirmed here. Any algal assemblage possessing SICF is theoretically detectable using this approach, while not taking into account complications introduced through variable fluorescence quantum yields between species, diel and other photo-physiological variations (Suggett et al., 2009).

A special case is encountered with low-medium biomass cyanobacteria-dominated algal assemblages. These blooms will not be detectable using a SICF approach, as cyanobacteria possess very inefficient SICF as most of the chl-*a* is located in photosystem I (Seppälä et al., 2007). An alternative approach is to take advantage of the phycocyanin fluorescence/absorption features visible in MERIS bands at 619 and 664 nm (see fig. 1.D). However, model studies show these features only become clearly distinguishable at chl-*a* concentrations larger than 8-10 mg.m^{-3}, assuming a SNR of 1000 or greater for the satellite sensor (Metsamaa et al., 2006). In this case, given a TOA type approach, these PC related features are probably only distinguishable at chl-*a* values larger than around 20-30 mg.m^{-3} (representing medium-high biomass) (Kutser et al., 2006). The ratio of PC:chl-*a* is also highly variable due to intracellular and physiological processes (Simis et al., 2005, 2007), rendering unsound chl-*a* estimates from PC related features. Therefore detection of cyano-bloom initiation may not be feasible with current instruments – for example, PC concentrations less than 50 mg.m^{-3} may not even be detected with confidence using *in situ* spectroradiometric data (Simis et al., 2007). It is also important to consider how frequently this special case scenario might occur in nature. Given that cyanobacteria have a strong tendency to become dominant in eutrophic high-biomass conditions, the risk of cyanobacterial dominance at chl-*a* < 20-30 mg.m^{-3} is small (Downing et al., 2001). For example, at chl-*a* concentrations < 10 mg.m^{-3}, the risk of cyanobacterial dominance is < 10%. Furthermore, the WHO alert level two gives a cyanobacterial chl-*a* concentration equal to or larger than 50 mg.m^{-3} for the issuing of cyanobacteria health warnings; however, this may drop to between 12-25 mg.m^{-3} for more toxic species (WHO, 1999). Given the above considerations, it is probably only possible, and arguably only necessary, to detect cyano-blooms of high biomass from an operational risk identification perspective. For these cases we can assume that the signal from absorption/backscatter related effects becomes apparent which, as now discussed, is the second case handled by the MPH algorithm.

4.2. The absorption/backscatter domain: high biomass eutrophic/hypertrophic waters

The second case for the MPH concerns high biomass eutrophic/hypertrophic water with chl-*a* concentrations greater than approx. 30 mg.m^{-3} (incidentally 30 mg.m^{-3} is the WHO classification threshold for eutrophic fresh water). These conditions are typically encountered in HAB affected systems during bloom periods. In this case, the red peak shifts towards longer wavelengths from the fluorescence peak at 681 nm (if present), to the phytoplankton backscatter-induced peak near 700 nm. In these phytoplankton dominant waters, chl-*a* is known to be highly correlated with the height (and position) of the 709 nm peak (Gitelson, 1992) and various algorithms have been designed to exploit this feature (e.g. Gitelson et al., 1993; Gons, 1999; Dall'Olmo & Gitelson, 2005; Zimba & Gitelson, 2006; Gitelson et al., 2009; Le et al., 2011). When the absorption/backscattering peak becomes more distinct than the fluorescence peak, the MPH is calculated using the 709 nm band and a baseline drawn between MERIS bands 7 and 14. This is similar to the scattered/reflectance line height algorithms (Dierberg & Carriker, 1994; Yacobi et al., 1995), and also the maximum chlorophyll index or MCI (Gower et al., 2005). Unfortunately, MERIS and OLCI are the only current and planned ocean colour sensors with appropriate bands near 700 nm able to utilise these types of algorithms.

4.3. A method for the discrimination of cyanobacteria-dominant waters

A simple but robust method for distinguishing high-biomass cyanobacteria-dominant waters from prokaryote dominant blooms is also implemented. The method is based on two theoretical and observable suppositions related to the unique pigment complement of cyanobacteria (section 3.2.2):

1. Cyanobacteria dominant waters possess no observable SICF peak at 681 nm (arrow 1, fig. 1.D)
2. Cyanobacteria dominant waters possess an observable SIPF peak at 664 nm (arrow 2, fig. 1.D)

Based on these observable features, it is possible to distinguish waters dominated by cyanobacteria (fig. 1.D) from those dominated by prokaryote chl-*a* fluorescing species (fig. 1.C). This presents itself in the MERIS waveband configuration by an observable trough at the 681 nm band, and an observable SIPF peak in the 664 nm band, respectively. Using the baseline subtraction technique, these two features are used to identify high biomass cyanobacteria dominant waters. The two baseline subtraction variables may be calculated as follows:

$$SICF_{peak} = \rho_{BR681} - \rho_{BR664} - ((\rho_{BR709} - \rho_{BR664}) \times (681 - 664)/(709 - 664)) \quad (2)$$

$$SIPF_{peak} = \rho_{BR664} - \rho_{BR619} - ((\rho_{BR681} - \rho_{BR619}) \times (664 - 619)/(681 - 619)) \quad (3)$$

The following condition, most easily expressed as a logical statement, is then used to raise a cyano-flag for the presence of cyano-dominance:

$$If\ SICF_{peak} < 0\ and\ SIPF_{peak} > 0,\ cyanoflag = TRUE \quad (4)$$

The cyano-flag correctly distinguished cyano-dominant water from those dominanted by prokaryote species in the dataset (fig. 1). However, for operational applications it is important to consider the detection limits of this kind of technique. As already shown for the special case related to low-biomass cyano-blooms, the PC fluorescence features may only be distinguishable at chl-*a* concentrations larger than 8-10 mg.m^{-3}, assuming a SNR of 1000 or larger for the satellite sensor (Metsamaa et al., 2006). In this case, using ρ_{BR} these features are probably only distinguishable at chl-*a* values larger than 20-30 mg.m^{-3} (Kutser et al., 2006).

4.4. Handling of cyanobacterial surface scums and floating vegetation

The third case handled by the MPH is extremely high biomass conditions associated with surface scums, or hyperscums, and dry floating algae or vegetation. Surface scums form during calm conditions as upwardly-buoyant algae (often cyanobacteria) accumulate on the water surface in dense mats or rafts. This is commonly observed, for example, in the coastal waters of the Gulf of Finland (Kutser, 2004), and in cyano-dominant lakes (Zohary, 1985; Hu et al., 2010b). In these extreme conditions, the red peak shifts towards 750 nm or higher wavelengths, because the absorbing effect of water is excluded or minimized. Consequently, the water leaving reflectance resembles dry vegetation rather than water (Richardson, 1996; Kutser, 2004; Kutser et al., 2009). For MERIS, the transition between a maximum peak position of 709 (band 9) and 754 nm (band 10) probably occurs at chl-*a* values close to or larger than 500 mg.m^{-3} (see fig. 3 in Kutser, 2004). Therefore, a flag is raised for surface scums using a threshold condition of chl-*a* > 500 mg.m^{-3} as a general classification (Kutser, 2004). This is because quantitative measures of chl-*a* in surface scum possesses much uncertainty as the dataset did not include any data within this range, and because surface scums have variable optical properties (Kutser et al., 2009).

Floating aquatic macrophytes, such as the notorious waterhyacinth *Eichhornia crassipes*, represent a substantial problem in inland waters. For example, water hyacinth is often present in Hartbeespoort dam in relatively small quantities, but can become widespread rapidly if not manually controlled using costly control measures (van Wyk & van Wilgen, 2002). Floating macrophytes have spectra resembling terrestrial dry vegetation (e.g. Cavalli et al., 2009) and may be detected by enlarged reflectance in the 754 nm band. In these instances where the maximum peak position is 754 nm, a flag is raised for floating vegetation. For these cases, the MPH resembles the floating algae index (FAI) algorithm used to detect floating surface scums in Lake Taihu, China with MODIS (Hu et al., 2010b). Quantitative chl-*a* estimation for floating vegetation detected by the MPH algorithm is not currently accounted for, although might be feasible following correct parameterisation on a species basis. The separation of land and water pixels also becomes more challenging when dealing with highly enlarged reflectance data in the NIR caused by floating macrophytes.

Cyanobacterial and prokaryotic surface scums were distinguished from one another using the cyano-flag from section 4.3. This is based on the assumption that the optical properties of the scums are not too deviant from algal cells in suspension. For pixels identified as cyanobacteria dominant and having either a chl-*a* value > 500 mg.m^{-3}, or a maximum peak position of 754 nm, a flag is raised for cyanobacterial scum (cyano-scum) . The presence of cyano-scum indicates a substantial risk for significant levels of toxin production. More than 50% of cyano-scums analysed in a sample of 50 scums in the U.K. were found to be toxic (Codd, 2000). Therefore, cyano-scums represent a substantial health risk. Since reflectance signatures from floating macrophytes do not possess the distinctive pigment-induced reflectance features of cyanobacteria, it is rather simple to distinguish between these and cyano-scum, using equation 4.

In summary, the MPH is designed to seamlessly handle low, medium and high biomass blooms, and surface scums occurring in HAB affected waters. In addition the MPH handles cyanobacteria dominant waters separately by distinguishing it from prokaryote blooms and floating vegetation. The MPH is trained using the combined dataset of 74 *in situ* chl-*a* observations with matching MERIS BRR spectra from the study areas. The spectra are each assigned class membership based on the position of the peak with the maximum height: the fluorescence domain (681 nm peak), the backscatter domain (709 nm peak), and the dry domain (753 nm peak). For each domain, a series of least squares fitting procedures correlated the observed matching *in situ* chl-*a* concentration with the MPH. In each case, the following functions were tested: exponential growth function of form $y = a \times exp(bx)$, quadratic function of form $y = ax^2 + bx + c$, power law function $y = ax^b$, and linear fit $y = a + bx$. The goodness of fit was in each case judged by the value of the root mean square error (rmse). The results of the analysis are presented in section 5.2.

5. Results and discussion

5.1. An analysis of adjacency effect corrections using ICOL+

To assess the effect of the ICOL correction, a comparison between AE corrected bottom-of-Rayleigh reflectances and uncorrected bottom-of-Rayleigh reflectances was performed (fig. 2). Some unusual and unexpected spectral shapes were obtained following correction with ICOL and these are illustrated using a few selected spectra (fig. 2.A). Against expectations, many of the corrected spectra showed elevated values at 885 nm and unusual shapes in the 753 − 778 nm region (compare to fig. 1). To gauge the overall effect of ICOL on the red bands, the mean percentage difference between uncorrected and corrected spectra was calculated (fig. 2.B). As expected, the effect of ICOL was to decrease the overall magnitude of the bands in the red. The mean percentage difference was -12.6% at 664 nm, -12.2% at 681 nm, -13.5% in at 709 nm, -10.7% at 753 nm and -5.2% at 885nm. ICOL had the greatest relative effect on the 709 nm band, while the effect further in the NIR is roughly half that. This result appears to be against expectations, given that other studies suggest that the adjacency effect is relatively larger in bands further towards the NIR (e.g. Odermatt et al., 2008). There is an expectation that bands further

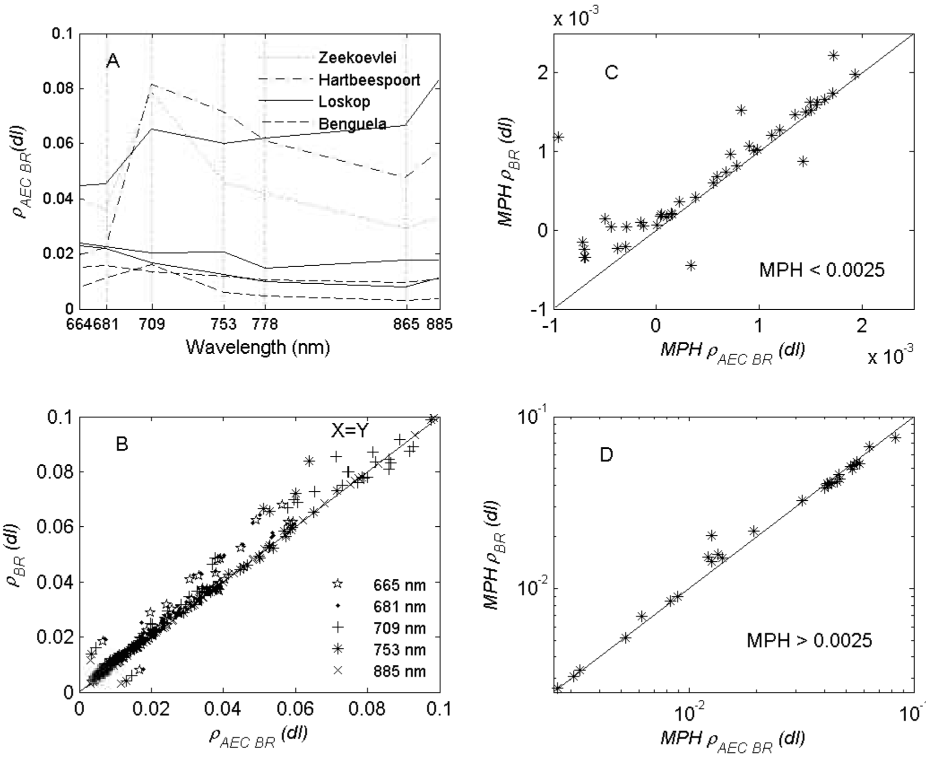

Figure 2: Comparison between uncorrected bottom-of-Rayleigh reflectances (ρ_{BR}) and those corrected for the adjacency effect using the ICOL+ processor (ρ_{AECBR}). Panel A shows selected spectra identified because of their unusual shapes following correction with ICOL. The change in the MERIS red bands following correction with ICOL is show in panel B. Similarly, panels C and D show the change in the MPH variable after application of ICOL, for low (C) and high ranges (D) of MPH.

towards the NIR have relatively larger correction factors. Therefore, there appears to be an overcorrection of smaller wavelengths (<709 nm) and an under-correction at larger wavelengths. Fig. 2.C and 2.D illustrate the effects of ICOL on the MPH variable (section 4.1). It was found that the height of the maximum peak in the red was reduced following ICOL by mean value of 12.0%, which had a significant effect on the value of the MPH variable. The MPH generally became smaller and there were more negative values (fig. 2.C). The mean percentage difference between the corrected/uncorrected MPH values was -47.2%, which was heavily influenced by a small number of large outliers.

Evidently, ICOL has a large influence on the MPH variable and significant effects on the red bands. ICOL was implemented in a way that calculates the aerosol type (that is the Angstrom coefficient (α)) and the aerosol optical thickness (AOT) over water while taking into account case 1 or case 2 water (based on the BRR at 709 nm). This means that the retrieval of the AOT and the aerosol type (α) is determined simultaneously from NIR bands and extrapolated to smaller MERIS bands (Santer, 2010). Therefore, the selection of an incorrect aerosol type could lead to the unusual effects (bias) observed in the ρ_{AECBR}. Therefore, the unexpected effects appear to be associated with the retrieval of the AOT and aerosol type selection. Based on these findings, an adjacency correction only taking into account Rayleigh effects is preferable, based on the recommendation of Santer & Schmechtig (2000) for operational AE corrections. The main reason for this is due to the large influence that the vertical aerosol distribution has on the aerosol AE, which is unknown. It seems that an AE correction including aerosol effects over these targets is currently not well performed and introduces artifacts in the data that cause more negative and erratic MPH values. Due to the sensitivity of the MPH to relative changes in the red/NIR bands and based on these initial analyses, ICOL+ is not recommended for application with the MPH algorithm at this stage. Undoubtedly, the small size and eutrophic conditions of the water targets makes them extremely challenging targets for any atmospheric or adjacency effect correction procedure.

5.2. Derivation of MPH

5.2.1. The fluorescence 681 nm domain

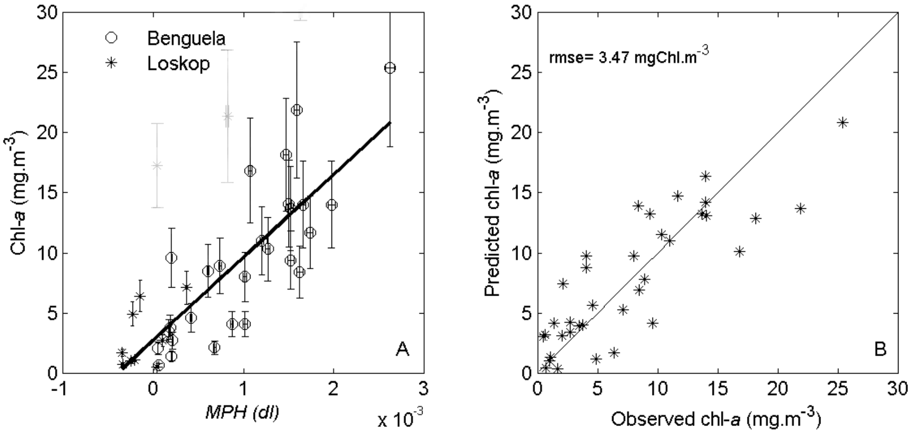

Figure 3: Chl-*a* versus the MPH for the fluorescence domain calculated using a maximum peak height position of 681 nm (panel A). Only data from Loskop and Benguela study areas belonged to this domain. Outliers are shown in grey. The observed chl-*a* versus that predicted by the MPH algorithm is shown in panel B.

Separate fits were used to best describe the fluorescence and absorption/backscatter domains. In the fluorescence domain the best fit was given as (fig. 3):

$$Chl\ a = 2.72 + 6903.13 \times MPH \quad (5)$$

The rmse is 3.5 mg.chl-a.m^{-3} and the mape is 69% for chl-a in the range 0.5 – 30 mg.m^{-3} (r^2 = 0.71, p = 0.00, F=83, N=36). Therefore the algorithm is sensitive to a minimum chl-a value of approximately 3.5 mg.m^{-3}. To improve the goodness of fit, the algorithm is constrained to data points with maximum peak positions at 681 nm and corresponding chl-a values < 30 mg.m^{-3}. This resulted in several outliers being excluded that had chl-a values > 30 mg.m^{-3} (N=3). This is because quantification of the fluorescence signal is challenging for chl-a values > 30 mg.m^{-3} Babin (1996), and to improve the algorithm's sensitivity at lower values. Further to this, outliers (show in grey on fig. 3) were also excluded from the regression, on the basis of a 95% confidence interval for studentized residuals (N=2). This also served to improve the goodness of fit.

Fig. 3 includes several data points with negative MPH values, all of which are from Loskop. These negative values are within the 95% confidence interval and occupy an expected region of low chl-a concentrations. For these reasons the data are not excluded. In determining an explanation for the negative MPH values, the specific conditions related to the target (Loskop), and the mechanisms whereby the MPH becomes inverted must be considered. Firstly, the data points are from the very dark oligotrophic main basin in Loskop lake. Atmospheric correction over similar, dark, oligotrophic lakes is extremely challenging due to stray light adjacency effects and the dark nature of the target (for the impact of the AE in subalpine lakes see Guanter et al., 2010; Odermatt et al., 2010). Such effects would cause reflectances in the red and NIR bands to be enlarged resulting in an inverted (negative) MPH. This seems to be the most plausible explanation for the negative values and highlights the difficulty associated with handling small, oligotrophic inland waters.

Despite this finding, the algorithm's performance in the florescence domain seems to be very robust given that it is capable of detecting chl-a with a sensitivity of less than 4 mg.m^{-3} from bottom-of-Rayleigh reflectance data. As fig. 3 shows, there were no data points from cyanobacteria dominant waters (Zeekoevlei/Hartbeespoort) belonging to the fluorescence domain. Table 2 shows statistics associated with the MPH variable used to determine discrete threshold values for the fluorescence domain.

5.2.2. The absorption/backscatter 709 nm domain

When plotting the absorption/backscatter domain, it immediately became apparent that there was a large offset in MPH values between data points from cyano-dominant waters (Zeekoevlei and Hartbeespoort) and those from prokaryote dominant waters (Loskop/Benguela) (fig. 4). Concurrently, there was excellent agreement between the data for each of these water types. Therefore, separate fits were used for cyano-dominant waters (eukaryotes) and for waters with phytoplankton assemblages made up predominately of dinoflagellates or diatoms (prokaryotes) (fig. 4.A). For dinoflagellate/diatom dominant waters, the best fit was given as:

$$Chl\ a = 37.18 + 11228.38 \times MPH \quad (6)$$

The rmse is 88.8 mg.m^{-3} which equates to a mean percentage error (mpe) of 104% (r^2=0.384, p=0.042, F=5.6). According to studentized residual values, there were no outliers. The algorithm was not constrained further due to the small sample number (N=11). The relatively low statistical significance and large mpe must be taken into account given the small sample size and the large

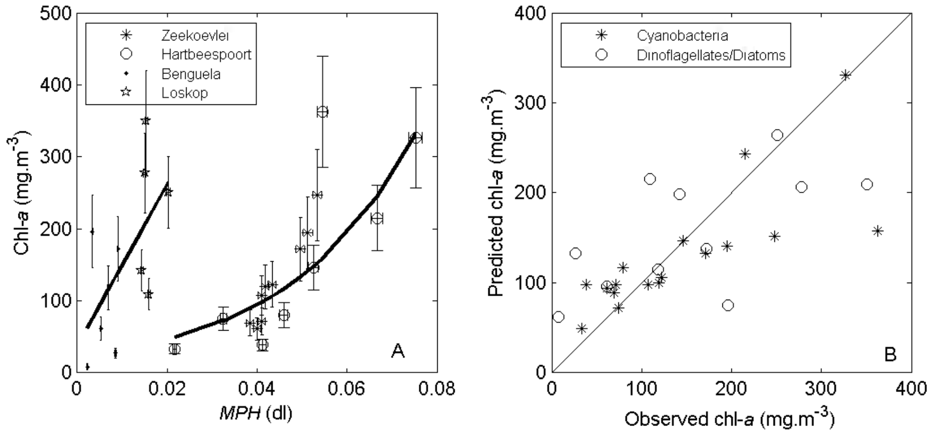

Figure 4: Performance of the MPH for the absorption/backscatter domain (panel A). Separate fits were used for cyano-dominant waters (Hartbeesport/Zeekoevlei) and prokaryote dominant waters (Loskop/Benguela). The observed vs. predicted chl-*a* is shown in panel B.

range of chl-*a* values over which the algorithm is expected to perform (a range of 343 mg.m^{-3}). An exponential fit was obtained for cyano-dominant waters:

$$Chl\ a = 22.44 \times exp(35.79 \times MPH) \tag{7}$$

The robust nonlinear least squares estimation gave an rmse of 46.6 mg.m^{-3} corresponding to a mape of 33.7% (r^2=0.58, N=17). All of the data from cyano-dominant waters had a 709 peak position and MPH values > 0.02 (see table 2). Based on the intercept of the algorithm, only chl-*a* values greater than 22.4 mg.m^{-3} can be estimated using the algorithm.

5.2.3. Theoretical considerations related to cyano-dominant waters

The large discontinuity in fig. 4 enables us to distinguish cyano-blooms purely on the basis of the magnitude of the MPH variable. These large and quantifiable differences in the red-NIR reflectance between prokaryote and eukaryote dominated waters requires closer examination. Assuming phytoplankton is the dominant constituent with regards to causal IOPs, the magnitude of the 709 nm peak will be dependent upon the specific backscattering coefficient (b_b*) of the dominant phytoplankton species, which is known to vary by several orders of magnitude between different species/classes (Whitmire et al., 2010; Stramski et al., 2001). Therefore, the large observed discontinuity could be explained on the basis that cyanobacteria (e.g. *Microcystis* sp.) have significantly greater backscattering per unit chl-*a* (chl-*a* specific backscatter coefficients, b_b*) in the red than dinoflagellate/diatom species. This would lead to larger MPH values such as observed in cyano-dominant waters since remote sensing reflectance is directly proportional to backscatter ($R \approx b_b/(a + b_b)$), while also providing a robust theoretical explanation for the observations. However, is there any evidence for this hypothesis?

Firstly, there is a significant amount of evidence that gas vacuoles found in certain cyanobacterial species (incl. *Microcystis aeruginosa*) are very efficient light scatterers in the forward and backward direction (Walsby, 1994). For example, in a turbid reservoir dominated by *Microcystis* spp., Ganf et al. (1989) found that 80% of light scatter could be attributed to the intracellular gas vacuoles. Further evidence can be found in the findings of Volten et al. (1998) who showed that the presence of gas vacuoles altered the scattering properties of phytoplankton considerably, in agreement with the earlier findings of Dubelaar et al. (1987) who found anomalous light scatter in vacuolate *Microcystis aeruginosa*. Because morphological differences and intracellular structure has been shown to have a large influence on backscattering (Whitmire et al., 2010; Svensen et al., 2007), the effect of gas vesicles in cyanobacterial cells on backscattering is likely to be substantial.

Secondly, phytoplankton with small diameters (d) possess larger backscatter per unit chl-*a* (b_b*) than intermediate and large celled species (Ahn et al., 1992; Bernard et al., 2009). Therefore, per unit chl-*a*, small celled cyanobacteria may backscatter up to two orders of magnitude greater than larger non-cyanobacterial species. Therefore, based on the presence of vacuoles, and on theoretical explanations and experimental observations related to cell size, cyanobacteria should in many instances posses larger b_b* than prokaryote species.

To verify whether this can be observed in natural waters, ancillary measurements of spectral backscattering collected using a Hydroscat 2 metre (Hobilabs Inc.) in *Microcystis aeruginosa* dominant blooms in Hartbeespoort and in a dense (chl-*a* > 500 mg.m^{-3}) dinoflagellate *Ceratium balechii* bloom in the southern Benguela (see Pitcher & Probyn, 2011) were used. The Hydroscat was configured to measure the backscattering coefficient at 420 and 700 nm. The conversion between the measured volume scattering function at 120 ° (minus pure water) to backscattering was based on a single conversion factor (χ) obtained from instrument calibration. A single conversion factor is known to be generally sufficient for use with various algal classes (e.g. Whitmire et al., 2010). From co-incident backscatter and chl-*a* measurements, a mean chl-*a* specific particulate backscatter ($b_{bp}*$) in Hartbeespoort was calculated as 0.4×10^{-3} m^{-1} at 420 nm and 1.98×10^{-3} m^{-1} at 700 nm (N = 13). In contrast, $b_{bp}*$ in the Benguela was 0.116×10^{-3} m^{-1} at 420 nm and 0.141×10^{-3} m^{-1} at 700 nm, an order or magnitude smaller than for *Microcystis*. These measurements, made in blooms when phytoplankton was demonstrably the dominant contributor to bulk IOPs, are within the range of those presented in Ahn et al. (1992) and Whitmire et al. (2010). If anything, the value for *Microcystis* is underestimated given that the measurements were made at a depth of 0.68 m and the blooms were floating. Nevertheless, the measurements reveal that for *Microcystis aeruginosa*, backscatter is slanted towards the red and is at least an order-of magnitude larger in the red than for the dinoflagellate *Ceratium balechii*.

Further conclusive evidence is found in Whitmire et al. (2010) who showed that for single species of cultured marine phytoplankton, there is a significant linear relationship between chl-*a* and b_{bp}, and that the magnitude and slope of b_{bp} is distinctive enough to distinguish between different species (see Fig. 5 in Whitmire et al., 2010). Substantial experimental and theoretical grounds therefore exist for the result in fig. 4. This might offer significant justification for the finding that cyano-blooms are distinguishable from non-cyanobacterial blooms based purely on the magnitude the absorption/backscatter-induced 709 nm peak, rather than on the observation of accessory pigment related reflectance features (such as those of phycocyanin). Given that the algal assemblages in our study areas were made up of comparative species, either *Microcystis aeruginosa* or *Ceratium* spp., the relationship between chl-*a* and b_{bp} was maintained between the systems, allowing derivation of algorithms specific for each of the algal classes.

5.3. An operational switching MPH algorithm

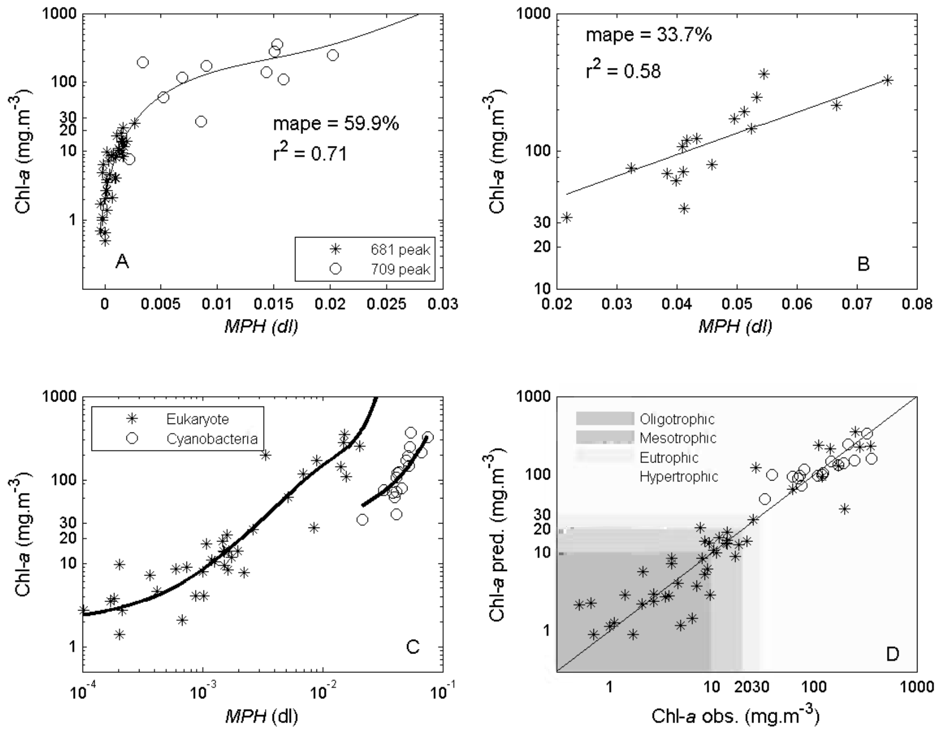

Figure 5: The switching operational MPH algorithm for prokaryote-dominant waters showing class membership (panel A). The MPH algorithm for cyano-dominant waters (panel B). The combined algorithms scope and performance is shown in panels C and D. Panel D shows the algorithms performance relative to trophic status classification.

Table 2: Statistics for the MPH variable grouped by the position of the maximum peak height.

Domain	Mean	Min.	Max.	Range	St. dev.	Chl-a min.	Chl-a max.
Fluorescence	0.00073	-0.00034	0.0026	0.00029	0.00078	0.5	26.85
Backscatter (dino/diatom)	0.0105	0.0022	0.0203	0.0180	0.0059	7.7	350.4
Backscatter (cyano)	0.0465	0.0217	0.0752	0.0536	0.0124	33.0	362.5

In order to obtain an algorithm suitable for operational use, a single algorithm for prokaryote algal assemblages and another for waters identified as cyano-dominant was developed. Table 2 shows the descriptive statistics for the MPH variable obtained from the statistical fits in figs. 3 and 4. The continuity between the fluorescence domain and the backscatter domain for prokaryotes is good, with some overlap. Therefore, in order to obtain a single continuous algorithm for chl-*a* estimation in prokaryote dominant waters, a 4th order polynomial was fitted after sorting the data (fig. 5) to obtain the following equation:

$$Chla(Prokaryotes) = 5.24\times10^{9}mph^{4} - 1.95\times10^{8}mph^{3} + 2.46\times10^{6}mph^{2} + 4.02\times10^{3}mph + 1.97 \quad (8)$$

The mean absolute percentage error of the algorithm is 59.9% and the r^2 value is 0.71. The operational algorithm is designed to operate seamlessly between the fluorescence and absorption/backscatter domains for prokaryote SICF possessing algae. Similar 4th order polynomials are also used for the operational empirical algorithms for MODIS (OC3M) (Campbell & Feng, 2005) and SeaWiFS (OC4) (O'Reilly et al., 1998), which use the maximum value of several band ratios, similar to the maximum peak selection of the MPH algorithm. The polynomial fit is advantageous because it provides good continuity between the different domains of the algorithm, shown in fig. 5.A. It is important to consider that the algorithm here is not the best fit for the data - the data has been sorted to give this fit - but rather the polynomial provides the smallest difference between predicted and observed chl-*a* values measured by the mean absolute percentage error (mape). For waters identified as cyanobacteria based on the flag in section 4.3, eq. 7 was used (fig. 5.B). The combined performance of the algorithms (fig. 5 C and D) in each of the trophic status classes is: oligotrophic, mape=71%, N=26; mesotrophic, mape=19%, N=9; eutrophic, mape= 131%, N=3; hypertrophic, mape=37%, N = 10.

6. Application and conclusions

6.1. Application to study areas

The operational MPH algorithm (section 5.3) was applied to imagery from the study areas in order to test its performance (fig. 6). The following cases were used to assess different aspects of the algorithm:

1. Identification of cyano-scums and cyano-dominant water in the hypertrophic waters of Hartbeespoort Dam.
2. Trophic status detection over a wide range of trophic states from oligotrophic to hypertrophic in prokaryotic-dominated assemblages in Loskop Dam.
3. High biomass HAB event detection in the waters of the southern Benguela and comparison with standard MERIS L2 algal products.

For the first test case, the cyano-flag correctly identified cyano-dominant water as well as cyano-scums that were observed at Hartbeespoort *in situ* during October 2010 (fig. 6.B). As a control, the algorithm was also applied to a scene from winter of the same year, before the onset of the spring cyano-bloom (fig. 6.A). In this case the algorithm did detect the presence of cyanobacteria in the lake, although this may be a result of chl-*a* concentrations below the detection limits of the cyano-flag (< 30 mg.m^{-3}). . Nevertheless, the example illustrates how the algorithm might be used for cyano-detection in small hypertrophic inland waters, and serve as a warning product for both commercial and recreational users. The cyano-flag also appeared robust when applied to a time series of the data (not shown here).

For the second test case, the MPH algorithm reproduced the strong longitudinal chl-*a* gradient observed *in situ* in Loskop during August of 2011 (fig 6.C). The hypertrophic water towards the riverine zone in the south west corner shows the presence of a persistent *Ceratium* dinoflagellate bloom, which was correctly identified as prokaryote-dominated (not cyanobacteria) by the algorithm. Towards the north east and the main basin of the lake, a gradual gradient is followed until oligotrophic water is found with chl-*a* less than 3 $mg.m^{-3}$. This demonstrates the algorithm's ability to operate over a large trophic range, switching smoothly between the 681 nm fluorescence and 709 nm absorption/backscatter-induced peaks as the optimal signal source. A second image from October 2011 shows that the bloom has moved further downstream towards the main basin of the lake most likely in response to the first spring rainfall. This example illustrates the capability of the MPH to operate across a wide range of trophic states in a small lake with some confidence and shows how the MPH might be used as a trophic status indicator in small inland waters.

The final test case is a high-biomass *Prorocentrum triestiunum* bloom that occurred in the southern Benguela during March 2005 (fig. 6.E, 6.F). Chl-*a* derived from the MPH algorithm correctly estimated the extremely high concentrations (> 300 $mg.m^{-3}$) that were observed *in situ* towards the coastline, and which occurred occasionally in dense patches (fig. 6.F). Comparatively, the standard MERIS L2 algal2 product (fig. 6.E) failed to reach these high concentrations, severely underestimating the bloom biomass. To achieve a more detailed comparison between the MPH algorithm derived chl-*a* and those from the standard MERIS algal1 and algal2 products, pixels were extracted from the rectangular boxes drawn in fig. 6.E, and scatter plots made (fig. 7). For waters with chl-*a* less than 25 $mg.m^{-3}$, the MPH estimates were found to be highly covariant ($r^2 = 0.93$) with the algal1 product. However, the MPH chl-*a* estimates were consistently and significantly larger than those from algal1 (fig. 7.A). This is likely a result of the lower sensitivity of the MPH algorithm, which is near a minimum of 3.5 $mg.m^{-3}$. The significant positive bias suggests that the MPH may overestimate chl-*a* in clear oligo/mesotrophic marine waters. This is expected given the dataset from which the algorithm is derived.

In waters surrounding the peak area of the bloom, chl-*a* estimates from the MPH algorithm were highly covariant with those from algal2 (r^2=0.88) when constrained to an upper range of 45 $mg.m^{-3}$ (fig. 7.B). Although chl-*a* from the MPH is positively biased, the values estimated in the range between $15 - 30$ $mg.m^{-3}$ are quite similar. For chl-*a* > 45 $mg.m^{-3}$, there was no correlation, since algal2 has an upper training range of around 30 $mg.m^{-3}$. However, the chl-*a* estimates > 45 $mg.m^{-3}$ neatly occupied an expected position on the graph indicating that that the MPH algorithm is operating well above the upper limits of algal2 which is unsuited to southern Benguela waters in bloom conditions.In summary, the MPH provides reasonable and stable comparisons with the MERIS L2 standard products, however, in this instance its usefulness appears to be limited to blooms with chl-*a* values larger than around 10 $mg.m^{-3}$, due to the algorithm's sensitivity. As there are currently no alternative quantitative ocean colour algorithms giving routine estimates > 30 $mg.m^{-3}$, no comparisons were possible inside this range. It remains to be seen how the MPH might compare with alternative ocean colour algorithms designed for extra high-biomass waters. Further testing of the algorithm using *in situ* data sets (such as NOMAD) is not feasible as these lack sufficient chl-*a* data from high biomass waters and reflectance data for the appropriate red/NIR reflectance bands required by the MPH algorithm.

6.2. Global application examples

The MPH algorithm was applied to various well-known study areas in order to demonstrate its cross-applicability for both cyanobacteria and floating algae detection in diverse environments. The Baltic sea is frequently affected by very large cyano-blooms in summer months that form surface scums, and these have often been observed using remote sensing (e.g. Reinart & Kutser, 2006). Fig 8.A. shows the MPH algorithm applied to a MERIS RR scene on 17 July 2002 (note RGB image alongside for comparison). The MPH correctly identifies the cyanobacterial bloom (shaded pixels) which are most likely *Aphanizomenon flos-aquae*, *Nodularia spumigena*, or *Anabaena circinalis*. This demonstrates the cyano-flag correctly identifies marine species of cyanobacteria in the Baltic sea. The range of chl-*a* values estimated by the algorithm are also within the ranges of those estimated by local algorithms for blooms occurring in the same month (Reinart & Kutser, 2006). Therefore initial results from the MPH algorithm indicates that it might be well-suited for application with cyano-blooms in the Baltic Sea, where conventional algorithms most often often fail.

Lake Taihu in China is well know for outbreaks of severe *Microcystis* spp. blooms that accumulate in dense cyano-scums on the surface. These have recently been observed in a ten year time series using MODIS and the floating algal index (FAI) (Hu et al., 2010a). Initial results from the MPH algorithm in Lake Taihu show that it correctly identifies these cyano-blooms and scums, reproducing the observations of Hu et al. (2010a) (fig. 8.B). This result is expected as the MPH algorithm is derived from lakes with *Microcystis* spp. dominated assemblages similar to Lake Taihu. As can be seen in the south eastern parts of the Lake, the MPH algorithm also detected floating macrophyte vegetation (magenta pixels). Macrophytes are know to occur in this region of the Lake and are most likely *Potamogetan maackianus* (pondweed) or *Vallisneria natans* (eelgrass) (Qin et al., 2007) which are emergent and floating-leaf species. A final example is given from Lake Victoria, which experiences severe eutrophication and cyano-dominance in some regions (e.g. Lung'ayia et al., 2000). Floating vegetation such as waterhyacinth (*Eichhornia crassipes*), Nile Cabbage (*Pistia stratiotes*), and water lily (*Nymphaea caerulea*) are also present in the Lake in standing crops (Cavalli et al., 2009). Fig 8.C. shows a MERIS FR scene indicating a large bloom identified as cyanobacteria, most likely *Microcystis* or *Anabaena* spp. (see Lung'ayia et al., 2000), extending into the central parts of the Lake, along with cyano-scum accumulations along the shoreline. This example, together with those above, demonstrate how the MPH algorithm and cyano-flag might be used for global monitoring of trophic status and cyano-blooms.

6.3. Conclusion

In conclusion, the MPH algorithm provides a new and efficient method for trophic status determination, cyano-bloom monitoring and floating vegetation detection in inland and coastal waters. The findings demonstrate that chl-*a* estimates for trophic status determination might be given with considerable accuracy using a top-of-atmosphere approach by taking advantage of absorption/backscatter and fluorescence related features in the red/NIR wavelengths of TOA reflectance data from the MERIS sensors. These features are clearly discernible in the TOA reflectance signal and the baseline-subtraction calculation of the MPH algorithm provides an effective normalisation of atmospheric effects, assuming that aerosol effects are not too spectrally deviant between the 664 and 885 nm bands. Therefore for broad trophic status assessment, simple Rayleigh atmospheric corrections are likely sufficient and avoid the more complicated and error-prone aerosol atmospheric corrections in turbid case II waters. The advantages of a

TOA-type approach are also evident in improved processing times and simpler implementation for operational monitoring systems.

The MPH variable presents itself as a suitable parameter for distinguishing prokaryotic phytoplankton from vacuolate cyanobacteria species. Large differences were observed in MPH magnitude between assemblages dominated by eukaryotic cyanobacteria *Microcystis* spp. (Zeekoevlei/Hartbeespoort) and prokaryotic dinoflagellates/diatoms (Benguela/Loskop). These differences allow for the discrimination of these algal classes in high biomass circumstances based on the magnitude of the MPH variable. This is substantiated by evidence that cyano-dominant waters have considerably higher backscatter per unit chl-*a* (b_b^*), leading to the increased magnitude of the MPH variable. This finding indicates the potential for 'tuning' of the MPH algorithm for various phytoplankton species using differences in the magnitude of chl-*a* specific backscatter (*cf.* Whitmire et al., 2010). Radiative transfer modeling studies will undoubtedly be valuable in confirming and further substantiating this finding, providing that appropriate parameterisations of the the relevant phase functions and IOPs are available. In addition, a flagging method was defined which allows cyano-dominant waters to be distinguished from other blooms on the basis of cyanobacteria-specific spectral pigmentation features related to enhanced SIPF and reduced SICF. Initial results from cases with coincident *in situ* observations, and examples from global applications, suggest that this flag is a robust method for detecting high-biomass occurrences of cyano-blooms (chl-*a* > 30 mg.m^{-3}). Further application of this technique will undoubtedly have significant implications for cyanobacteria-oriented early warning remote sensing systems, as well as for frequency/risk analysis applications and bloom phenology.

The uncertainties related to the chl-*a* algorithms originate from the 'single point' sampling error, chl-*a* quantification methods, and atmospheric and sub-pixel variability. Notwithstanding the relatively small magnitudes of these errors, chl-*a* estimates are likely confident to within 3.5 mg.m^{-3} for chl-*a* < 30, and > 50 mg.m^{-3} for chl-*a* < 500 mg.m^{-3}. Detection of cyano-bloom initiation (< 30 mg.m^{-3}) remains challenging due to a lack of appropriate signal caused by a relative absence of SICF. Low-biomass waters having high mineral content also present a challenge due to interference with the SICF signal (Mckee et al., 2007). Therefore, the MPH algorithm is best suited for application in waters where phytoplankton is the dominant contributor to the bulk IOPs.

The MPH algorithm presents a new approach for empirical algorithms estimating chl-*a* in inland and coastal waters. This is one of only a few studies showing that empirical chl-*a* measurements are significantly correlated with a variable derived from top-of-atmosphere MERIS reflectance data (see also Giardino et al., 2005; Matthews et al., 2010). Furthermore, this is the first study where cyano-dominant waters have conclusively been distinguished from prokaryote-dominant algal assemblages on the basis of variable chl-*a* specific backscatter as observed in the 709 nm peak in MERIS band 9. This finding has substantial implications for empirical and model-based algorithms aimed at identifying algal classes in eutrophic waters from space. A new technique presented for cyanobacteria detection based on cyanobacteria-specific spectral pigmentation and fluorescence features should provide more information on cyano-dominance in inland and coastal waters. In conclusion, the MPH algorithm is useful for estimating trophic status, cyano-dominance, and the occurrence of surface scums and floating vegetation, and presents a substantial opportunity for monitoring systems aimed at filling information gaps on the severity and extent of these problems in inland and coastal waters. The routine generation of such products will have a broad range of conservation, trend analysis, status determination, quality auditing and ecosystem analysis applications.

7. Acknowledgments

The authors would like to express their sincere thanks to the following people for their assistance with data collection: Grant Pitcher and Trevor Probyn, Department of Agriculture, Fisheries and Forestry (DAFF); Nadene Slabbert, Department of Water Affairs; Paul Oberholster, Nobuhle Majozi, Heidi van Deventer and Jackie Brown, CSIR; Jannie Coetzee and Hannes Botha, Mpumalanga Tourism and Parks Agency; Asieff Khan, City of Cape Town; the Applied Behavioural Ecology and Ecosystem Research Unit. We would also like to thank the CSIR and the University of Cape Town for funding assistance.

References

ACRI (2006). *MERIS Level 2 Detailed Processing Model*. Technical Report 7.

Ahn, Y. H., Bricaud, A., & Morel, A. (1992). Light backscattering efficiency and related properties of some phytoplankters. *Deep-Sea Research*, *39*, 1835.

Babin, M. (1996). Remote sensing of sea surface Sun-induced chlorophyll fluorescence: consequences of natural variations in the optical characteristics of phytoplankton and the quantum yield of chlorophyll a fluorescence. *International Journal of Remote Sensing*, *17*, 2417–2448.

Bernard, S., Probyn, T. A., & Barlow, R. G. (2001). Measured and modelled optical properties of particulate matter in the southern Benguela. *South African Journal of Science*, *97*, 410–420.

Bernard, S., Probyn, T. a., & Quirantes, a. (2009). Simulating the optical properties of phytoplankton cells using a two-layered spherical geometry. *Biogeosciences Discussions*, *6*, 1497–1563.

Binding, C., & Greenberg, T. (2011). An assessment of MERIS algal products during an intense bloom in Lake of the Woods. *Journal of Plankton Research*, *33*, 793–806.

Bogorad, L. (1975). Phycobiliproteins and complementary chromatic adaptation. *Annual review of plant physiology*, *26*, 369–401.

Bouvet, M., & Ramoino, F. (2009). *Equalization of MERIS L1b products from the 2nd reprocessing*. Technical Report 1 European Space Agency.

Campbell, J. W., & Feng, H. (2005). The empirical chlorophyll algorithm for MODIS: Testing the OC3M algorithm using NOMAD data. In *Ocean Color Bio-optical Algorithm Mini-workshop, 27 - 29 September 2005* (pp. 1–9). Durham, New Hampshire: NASA.

Cavalli, R. M., Laneve, G., Fusilli, L., Pignatti, S., & Santini, F. (2009). Remote sensing water observation for supporting Lake Victoria weed management. *Journal of environmental management*, *90*, 2199–211.

Codd, G. A. (2000). Cyanobacterial toxins, the perception of water quality, and the prioritisation of eutrophication control. *Ecological Engineering*, *16*, 51–60.

Dall'Olmo, G., & Gitelson, A. a. (2005). Effect of bio-optical parameter variability on the remote estimation of chlorophyll-a concentration in turbid productive waters: experimental results. *Applied Optics*, *44*, 412–422.

Dierberg, F. E., & Carriker, N. E. (1994). Field testing two instruments for remotely sensing water quality in the Tennessee Valley. *Environmental science & technology*, *28*, 16–25.

Downing, J. A., Watson, S. B., & McCauley, E. (2001). Predicting Cyanobacteria dominance in lakes. *Canadian Journal of Fisheries and Aquatic Sciences*, *58*, 1905–1908.

Dubelaar, G. B., Visser, J. W., & Donze, M. (1987). Anomalous behaviour of forward and perpendicular light scattering of a cyanobacterium owing to intracellular gas vacuoles. *Cytometry*, *8*, 405–12.

Ducklow, H., & Dickson, A. (1994). Chapter 14. Measurement of Chlorophyll a and Paeopigments by Fluorometric Analysis. *JGOFS Protocols*, (pp. 119–122).

Fawcett, A., Pitcher, G., Bernard, S., Cembella, A., & Kudela, R. (2007). Contrasting wind patterns and toxigenic phytoplankton in the southern Benguela upwelling system. *Marine Ecology Progress Series*, *348*, 19–31.

Galat, D., & Verdin, J. (1989). Patchiness, collapse and succession of a cyanobacterial bloom evaluated by synoptic sampling and remote sensing. *Journal of Plankton Research*, *11*, 925–948.

Ganf, G. G., Oliver, R. L., & Walsby, A. E. (1989). Optical properties of gas-vacuolate cells and colonies of Microcystis in relation to light attenuation in a turbid, stratified reservoir (Mount Bold Reservoir, South Australia). *Australian Journal of Marine and Freshwater Research*, *40*, 595–611.

Giardino, C., Candiani, G., & Zilioli, E. (2005). Detecting Chlorophyll-a in Lake Garda Using TOA MERIS Radiances. *Photogrammetric Engineering & Remote Sensing*, *71*, 1045–1051.

Gitelson, A. (1992). The peak near 700 nm on radiance spectra of algae and water: relationships of its magnitude and position with chlorophyll concentration. *International Journal of Remote Sensing*, *13*, 3367–3373.

Gitelson, A., Garbuzov, G., Szilagyi, F., Mittenzwey, K. H., Karnieli, A., & Kaiser, A. (1993). Quantitative remote sensing methods for real-time monitoring of inland waters quality. *International Journal of Remote Sensing*, *14*, 1269–1295.

Gitelson, A., Mayo, M., Yacobi, Y. Z., Parparov, A., & Berman, T. (1994). The use of high-spectral-resolution radiometer data for detection of low chlorophyll concentrations in Lake Kinneret. *Journal of Plankton Research*, *16*, 993–1002.

Gitelson, A. A., Dall'Olmo, G., Moses, W., Rundquist, D. C., Barrow, T., Fisher, T. R., Gurlin, D., & Holz, J. (2008). A simple semi-analytical model for remote estimation of chlorophyll-a in turbid waters: validation. *Remote Sensing of Environment*, *112*, 3582–3593.

Gitelson, A. A., Gurlin, D., Moses, W. J., & Barrow, T. (2009). A bio-optical algorithm for the remote estimation of the chlorophyll-a concentration in case 2 waters. *Environmental Research Letters*, *4*, 45003.

Gons, H., Auer, M., & Effler, S. (2008). MERIS satellite chlorophyll mapping of oligotrophic and eutrophic waters in the Laurentian Great Lakes. *Remote Sensing of Environment*, *112*, 4098–4106.

Gons, H. J. (1999). Optical teledetection of chlorophyll a in turbid inland waters. *Environmental science & technology*, *33*, 1127–1132.

Gons, H. J. (2005). Effect of a waveband shift on chlorophyll retrieval from MERIS imagery of inland and coastal waters. *Journal of Plankton Research*, *27*, 125–127.

Gons, H. J., Rijkeboer, M., & Ruddick, K. G. (2002). A chlorophyll-retrieval algorithm for satellite imagery (Medium Resolution Imaging Spectrometer) of inland and coastal waters. *Journal of Plankton Research*, *24*, 947–951.

Gower, J., & King, S. (2007). Validation of chlorophyll fluorescence derived from MERIS on the west coast of Canada. *International Journal of Remote Sensing*, *28*, 625–635.

Gower, J., King, S., Borstad, G., & Brown, L. (2005). Detection of intense plankton blooms using the 709 nm band of the MERIS imaging spectrometer. *International Journal of Remote Sensing*, *26*, 2005–2012.

Gower, J. F. R. (1980). Observations of in situ fluorescence of chlorophyll-a in Saanich Inlet. *Boundary-Layer Meteorology*, *18*, 235–245.

Gower, J. F. R., Doerffer, R., & Borstad, G. A. (1999). Interpretation of the 685nm peak in water-leaving radiance spectra in terms of fluorescence, absorption and scattering, and its observation by MERIS. *International Journal of Remote Sensing*, *20*, 1771–1786.

Guanter, L., Ruiz-Verdú, A., Odermatt, D., Giardino, C., Simis, S., Estellés, V., Heege, T., Domínguez-Gómez, J. A., & Moreno, J. (2010). Atmospheric correction of ENVISAT/MERIS data over inland waters: Validation for European lakes. *Remote Sensing of Environment*, *114*, 467–480.

Harding, W. R. (1997). Phytoplankton primary production in a shallow, well-mixed, hypertrophic South African lake. *Hydrobiologia*, *344*, 87–102.

Hoge, F. E., Lyon, P. E., Swift, R. N., Yungel, J. K., Abbott, M. R., Letelier, R. M., & Esaias, W. E. (2003). Validation of Terra-MODIS Phytoplankton Chlorophyll Fluorescence Line Height. I. Initial Airborne Lidar Results. *Applied Optics*, *42*, 2767.

Holm-Hansen, O., Lorenzen, C. J., Holmes, R. W., & Strickland, J. D. H. (1965). Fluorometric Determination of Chlorophyll. *Journal du Conseil*, *30*, 3.

Hu, C., Cannizzaro, J., Carder, K. L., Muller-Karger, F. E., & Hardy, R. (2010a). Remote detection of Trichodesmium blooms in optically complex coastal waters: Examples with MODIS full-spectral data. *Remote Sensing of Environment*, *114*, 2048–2058.

Hu, C., Lee, Z., Ma, R., Yu, K., Li, D., & Shang, S. (2010b). Moderate Resolution Imaging Spectroradiometer (MODIS) observations of cyanobacteria blooms in Taihu Lake, China. *Journal of Geophysical Research*, *115*, 1–20.

Kutser, T. (2004). Quantitative detection of chlorophyll in cyanobacterial blooms by satellite remote sensing. *Limnology and Oceanography*, *49*, 2179–2189.

Kutser, T. (2009). Passive optical remote sensing of cyanobacteria and other intense phytoplankton blooms in coastal and inland waters. *International Journal of Remote Sensing*, *30*, 4401–4425.

Kutser, T., Metsamaa, L., Strömbeck, N., & Vahtmäe, E. (2006). Monitoring cyanobacterial blooms by satellite remote sensing. *Estuarine, Coastal and Shelf Science*, *67*, 303–312.

Kutser, T., Paavel, B., & Metsamaa, L. (2009). Mapping coloured dissolved organic matter concentration in coastal waters. *International Journal of Remote Sensing*, *30*, 5843–5849.

Le, C., Li, Y., Zha, Y., Sun, D., Huang, C., & Zhang, H. (2011). Remote estimation of chlorophyll a in optically complex waters based on optical classification. *Remote Sensing of Environment*, *115*, 725–737.

Lee, Z., Hu, C., Gray, D., Casey, B., Arnone, R., Weidemann, A., Ray, R., & Goode, W. (2007). Properties of coastal waters around the US: preliminary results using MERIS data. In *Proc. Envisat Symposium, 2327 April 2007* c. Montreux, Switzerland: ESA SP-636.

Letelier, M., & Abbott, M. R. (1996). An analysis of chlorophyll fluorescence algorithms for the moderate resolution imaging spectrometer (MODIS). *Remote Sensing of Environment*, *58*, 215–223.

Lung'ayia, H. B. O., M'harzi, A., Tackx, M., Gichuki, J., & Symoens, J. J. (2000). Phytoplankton community structure and environment in the Kenyan waters of Lake Victoria. *Freshwater Biology*, *43*, 529–543.

Matthews, M. W. (2011). A current review of empirical procedures of remote sensing in inland and near-coastal transitional waters. *International Journal of Remote Sensing*, *32*, 6855–6899.

Matthews, M. W., Bernard, S., & Winter, K. (2010). Remote sensing of cyanobacteria-dominant algal blooms and water quality parameters in Zeekoevlei, a small hypertrophic lake, using MERIS. *Remote Sensing of Environment*, *114*, 2070–2087.

Mckee, D., Cunningham, A., Wright, D., & Hay, L. (2007). Potential impacts of nonalgal materials on water-leaving Sun induced chlorophyll fluorescence signals in coastal waters. *Applied Optics*, *46*, 7720–7729.

Metsamaa, L., Kutser, T., & Stroembeck, N. (2006). Recognising cyanobacterial blooms based on their optical signature: a modelling study. *Boreal Environment Research*, *11*, 493–506.

Moses, W., Gitelson, A., Berdnikov, S., & Povazhnyy, V. (2009a). Satellite estimation of chlorophyll-a concentration using the red and NIR bands of MERISthe Azov Sea case study. *IEEE Geoscience and Remote Sensing Letters*, *6*, 845–849.

Moses, W. J., Gitelson, A. A., Berdnikov, S., & Povazhnyy, V. (2009b). Estimation of chlorophyll-a concentration in case II waters using MODIS and MERIS datasuccesses and challenges. *Environmental Research Letters*, *4*, 45005.

Neville, R. a., & Gower, J. F. R. (1977). Passive Remote Sensing of Phytoplankton via Chlorophyll α Fluorescence. *Journal of Geophysical Research*, *82*, 3487–3493.

Oberholster, P. J., Myburgh, J. G., Ashton, P. J., & a M Botha (2010). Responses of phytoplankton upon exposure to a mixture of acid mine drainage and high levels of nutrient pollution in Lake Loskop, South Africa. *Ecotoxicology and environmental safety*, *73*, 326–35.

Odermatt, D., Giardino, C., & Heege, T. (2010). Chlorophyll retrieval with MERIS Case-2-Regional in perialpine lakes. *Remote Sensing of Environment*, *114*, 607–617.

Odermatt, D., Kiselev, S., Heege, T., Kneubühler, M., & Itten, K. I. (2008). Adjacency effect consideration a and air/water constituent retrieval for Lake Constance. In ESA/ESRIN (Ed.), *Proceedings of the 2nd MERIS/(A)ATSR user workshop. Frascati, Italy* 1.

O'Reilly, J. E., Maritorena, S., Mitchell, B. G., Siegel, D. A., Carder, K. L., Garver, S. A., Kahru, M., & McClain, C. (1998). Ocean color chlorophyll algorithms for SeaWiFS. *Journal of Geophysical Research*, *103*, 24937–24953.

Pitcher, G. C., & Calder, D. (2000). Harmful algal blooms of the southern Benguela current: a review and appraisal of monitoring from 1989 to 1997. *South African Journal of Marine Science*, *22*, 255–271.

Pitcher, G. C., & Probyn, T. A. (2011). Anoxia in southern Benguela during the autumn of 2009 and its linkage to a bloom of the dinoflagellate Ceratium balechii. *Harmful Algae*, *11*, 23–32.

Pitcher, G. C., & Weeks, S. J. (2006). The variability and potential for prediction of harmful algal blooms in the southern Benguela ecosystem. *Large Marine Ecosystems*, *14*, 125–146.

Qin, B., Xu, P., Wu, Q., Luo, L., Zhang, Y., Qin, B., Liu, Z., Havens, K., & Dumont, H. J. (2007). *Eutrophication of Shallow Lakes with Special Reference to Lake Taihu, China* volume 194 of *Developments in Hydrobiology*. Dordrecht: Springer Netherlands.

Reinart, A., & Kutser, T. (2006). Comparison of different satellite sensors in detecting cyanobacterial bloom events in the Baltic Sea. *Remote Sensing of Environment*, *102*, 74–85.

Richardson, L. L. (1996). Remote Sensing of Algal Bloom Dynamics. *Bioscience*, *46*, 492–501.

Robarts, R., & Zohary, T. (1992). The influence of temperature and light on the upper limit of Microcystis aeruginosa production in a hypertrophic reservoir. *Journal of Plankton Research*, *14*, 235.

Robarts, R. D., & Zohary, T. (1984). Microcystis aeruginosa and underwater light attenuation in a hypertrophic lake (Hartbeespoort Dam, South Africa). *Journal of Ecology*, *72*, 1001–1017.

Santer, R. (2010). *ICOL+ Algorithm Theoretical Basis Document*. Technical Report V1.0 Brockmann Consult.

Santer, R., Carrere, V., Dubuisson, P., & Roger, J. (1999). Atmospheric correction over land for MERIS. *International Journal of Remote Sensing*, *20*, 1819–1840.

Santer, R., & Schmechtig, C. (2000). Adjacency effects on water surfaces: primary scattering approximation and sensitivity study. *Applied Optics*, *39*, 361–375.

Sartory, D. P., & Grobbelaar, J. U. (1984). Extraction of chlorophyll a from freshwater phytoplankton for spectrophotometric analysis. *Hydrobiologia*, *114*, 177–187.

Schalles, J. F., Gitelson, A. A., Yacobi, Y. Z., & Kroenke, A. E. (1998). Estimation of chlorophyll a from time series measurements of high spectral resolution reflectance in an eutrophic lake. *Journal of Phycology*, *34*, 383–390.

Schiller, H., & Doerffer, R. (2005). Improved determination of coastal water constituent concentrations from MERIS data. *IEEE Transactions on Geoscience and Remote Sensing*, *43*, 1585–1591.

Seppälä, J., Ylöstalo, P., Kaitala, S., Hällfors, S., Raateoja, M., & Maunula, P. (2007). Ship-of-opportunity based phycocyanin fluorescence monitoring of the filamentous cyanobacteria bloom dynamics in the Baltic Sea. *Estuarine, Coastal and Shelf Science*, *73*, 489–500.

Simis, S. G. H., Peters, S. W. M., & Gons, H. J. (2005). Remote sensing of the cyanobacterial pigment phycocyanin in turbid inland water. *Limnology and Oceanography*, *50*, 237–245.

Simis, S. G. H., Ruiz-Verdu, A., Dominguez-Gomez, J. A., Pena-Martinez, R., Peters, S. W. M., & Gons, H. J. (2007).

Influence of phytoplankton pigment composition on remote sensing of cyanobacterial biomass. *Remote Sensing of Environment*, *106*, 414–427.

Sotis, G. (2007). *Envisat-1 Products Specifications Volume 11: MERIS Products Specifications*. Technical Report 5 B.

Stramski, D., Bricaud, A., & Morel, A. (2001). Modeling the inherent optical properties of the ocean based on the detailed composition of the planktonic community. *Applied Optics*, *40*, 2929–2945.

Suggett, D., Moore, C., Hickman, A., & Geider, R. J. (2009). Interpretation of fast repetition rate(FRR) fluorescence: signatures of phytoplankton community structure versus physiological state. *Marine Ecology Progress Series*, *376*, 1–19.

Svensen, O., Frette, O., & Erga, S. R. (2007). Scattering properties of microalgae: the effect of cell size and cell wall. *Applied Optics*, *46*, 5762–5769.

Volten, A. H., Haan, J. F. D., Hovenier, J. W., Schreurs, R., Vassen, W., Dekker, A. G., Hoogenboom, J., Charlton, F., & Wouts, R. (1998). Laboratory Measurements of Angular Distributions of Light Scattered by Phytoplankton and Silt. *Limnology and Oceanography*, *43*, 1180–1197.

Walsby, A. E. (1994). Gas vesicles. *Microbiological reviews*, *58*, 94–144.

Whitmire, A. L., Pegau, W. S., Karp-boss, L., Boss, E., & Cowles, T. J. (2010). Spectral backscattering properties of marine phytoplankton cultures. *Optics Express*, *18*, 1680–1690.

WHO (1999). *Toxic Cyanobacteria in Water: A guide to their public health consequences, monitoring and management*. London: E & FN Spon.

van Wyk, E., & van Wilgen, B. W. (2002). The cost of water hyacinth control in South Africa : a case study of three options. *African Journal of Aquatic Science*, *27*, 141–149.

Yacobi, Y. Z., Gitelson, A., & Mayo, M. (1995). Remote sensing of chlorophyll in Lake Kinneret using high spectral-resolution radiometer and Landsat TM: spectral features of reflectance and algorithm development. *Journal of Plankton Research*, *17*, 2155–2173.

Zhao, J., Cao, W., Yang, Y., Wang, G., Zhou, W., & Sun, Z. (2008). Measuring natural phytoplankton fluorescence and biomass: A case study of algal bloom in the Pearl River estuary. *Marine pollution bulletin*, *56*, 1795–1801.

Zimba, P. V., & Gitelson, A. (2006). Remote estimation of chlorophyll concentration in hyper-eutrophic aquatic systems: Model tuning and accuracy optimization. *Aquaculture*, *256*, 272–286.

Zohary, T. (1985). Hyperscums of the cyanobacterium Microcystis aeruginosa in a hypertrophic lake (Hartbeespoort Dam, South Africa). *Journal of Plankton Research*, *7*, 399.

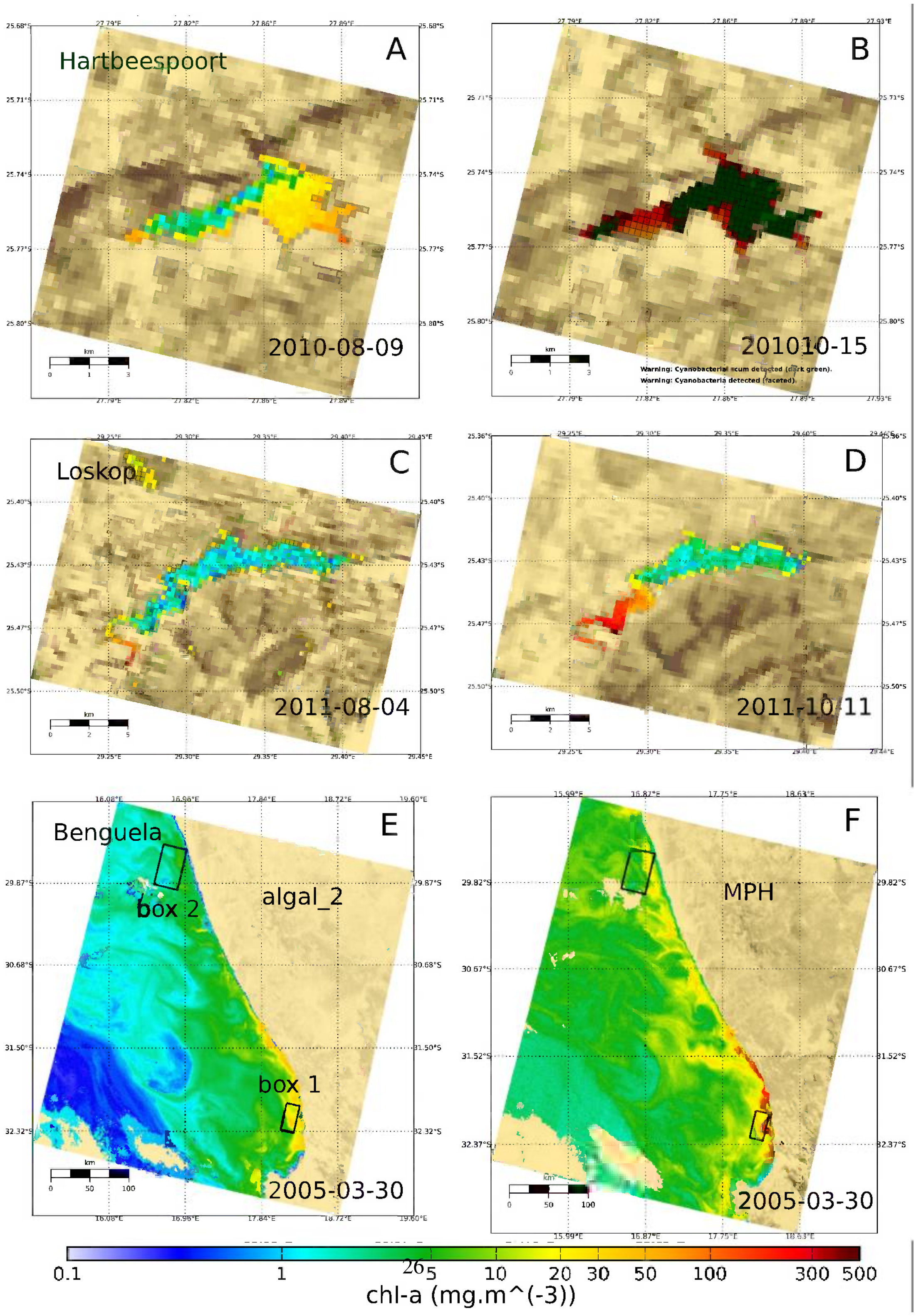

Figure 6: Example applications of MPH V. 1.0 to Hartbeespoort Dam (A, B) Loskop Dam (C, D) and the southern Benguela (E, F). Shaded and faceted pixels indicate where the flag for cyanobacteria has been raised while dark green pixels indicate surface scum (chl-*a* > 500 mg.m^{-3}). Box 1 shows the pixels extracted for comparison with the algal2 product, while box 2 shows those extracted for comparison with algal1.

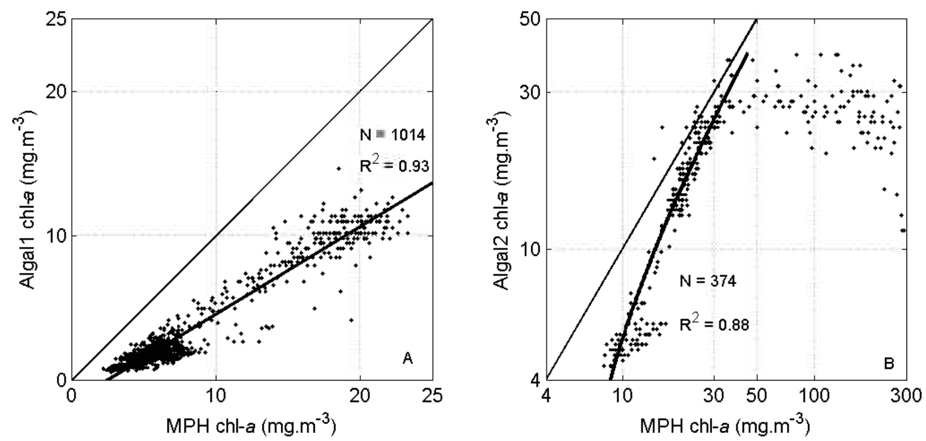

Figure 7: Comparison between MERIS standard level 2 products, algal1 (panel A) and algal2 (panel B) and chl-*a* derived from MPH in the southern Benguela in a large dinoflagellate bloom on 30 March 2005. The boxes in fig. 6 show where the data was taken from within the scene.

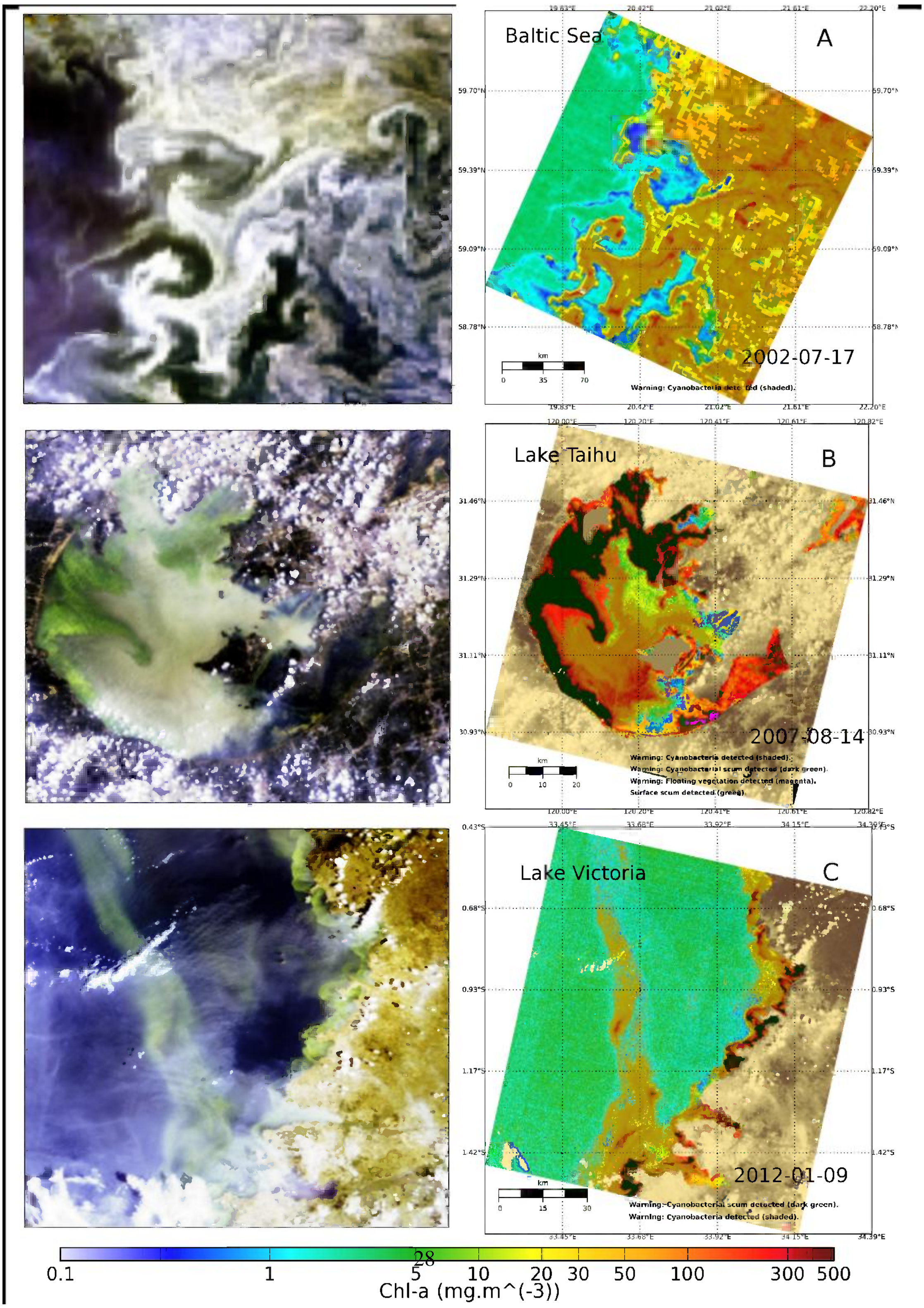

Figure 8: Global examples of the MPH in A) the Baltic sea during and intense cyanobacteria bloom (likely *Aphanizomenon flos-aquae*), B) Lake Taihu (*Microcystis aeruginosa*), and C) Lake Victoria (unidentified species). Pixels with shading indicate where cyanobacteria is detected with certainty. RGB images are shown alongside for comparison.